Journal of Sound and Vibration 329 (2010) 2147–2157

Contents lists available at ScienceDirect

Journal of Sound and Vibration

journal homepage: www.elsevier.com/locate/jsvi

Two-dimensional frequency domain scattering and point excitation of partially filled elastic cylinders

Samuel D.M. Adams [a], Richard V. Craster [a,b,*], Duncan P. Williams [c]

[a] Department of Mathematics, Imperial College London, South Kensington Campus, London SW7 2AZ, UK
[b] Department of Mathematical and Statistical Sciences, University of Alberta, Edmonton, Canada T6G 2G1
[c] Defence Science and Technology Laboratory, Physical Sciences, Porton Down, Salisbury SP4 0JQ, UK

ARTICLE INFO

Article history:
Received 19 January 2009
Received in revised form
23 December 2009
Accepted 3 January 2010
Handling Editor: R.J. Astley
Available online 27 January 2010

ABSTRACT

A suite of problems involving solid–fluid interactions with a two-dimensional cylindrical structure, i.e. with non-oblique forcing or wave incidence, is considered. Assessments are made of how the amount of filling in the interior effects the external response of the cylinder both qualitatively and quantitatively, with a view to developing long-range non-destructive testing techniques for submerged part-filled objects. Resonance frequencies are found and their usefulness, or otherwise, in characterising the extent of inner filling fraction. Numerical algorithms are generated to grid the domain and are complemented by a discussion of the use of perfectly matched layers to model the infinite background fluid; it is demonstrated that it is preferable not to directly attach the layer directly to the cylinder.

1. Introduction

There is a long-standing interest in the acoustical response of elastic objects and the countless tasks that rely on this response. The reader will be familiar with the use of sonar to search for underwater objects such as submarines and mines. Elsewhere, the non-invasive testing of containers is used to inspect and characterise their contents in applications such as the identification of unexploded ordnance [1] or cargo screening. Recent events have shown that reliable means to identify explosives and weapons, or other contraband and suspicious materials, and even stowaways, hidden inside containers would be just as welcome to port authority and airport security operations.

It is for these reasons that the properties of both, cylindrical and spherical, shells which are completely filled with fluid, or immersed within a fluid, or both, have been widely studied [2]. For example, the acoustic excitation of such shells, or similar structures, in response to either long or short range testing, has been the subject of intensive scientific investigation for the past 50 years [3,4]. Despite this, cylindrical or spherical shells containing an arbitrary amount of filling are far less well studied other than some notable and recent exceptions [5–8]. The relative lack of information on the response of arbitrarily filled objects can cause problems in reliably discriminating between objects or when trying to inspect the interior of objects such as containers. In some cases, this can lead to an inappropriate decision, or action, being taken.

Previous investigations of this problem have been limited to specific configurations, either of the quantity and nature of the filling, or on the geometry of the problem including the incident field. Here we are explicitly looking at how the

* Corresponding author at: Department of Mathematical and Statistical Sciences, University of Alberta, Edmonton, Canada T6G 2G1.
E-mail address: craster@ualberta.ca (R.V. Craster).

0022-460X/$ - see front matter © 2010 Elsevier Ltd. All rights reserved.
doi:10.1016/j.jsv.2010.01.007

response of the cylinder changes with the level of filling, between empty and completely filled, for cylinders submerged in different fluids, with point or plane wave forcing, together with variations in observation angle and/or position.

Empty or fully filled cylinders, or shells, are relatively straightforward to model: their solutions are separable in a polar coordinate system centred on the axis of the cylinder and Bessel function expansions generate exact dispersion relations [9,10]. Additionally, a wide range of numerical techniques are on offer: one can use finite differences, in which uniform grids in radial and angular directions are the obvious choice, and implementation requires only a basic understanding of the method, or alternatively, one can use spectral collocation for which efficient pre-written algorithms for weight generation exist [11]. The main numerical challenge is in dealing with submerged structures, as the modelling of an infinite fluid requires the use of an absorbing boundary condition, such as the perfectly matched layer [12] (PML), as used in this text.

By contrast, a study of arbitrarily filled objects imposes greater challenges, which limit the spectrum of available methods. The coordinate system is no longer neatly separable and Bessel function expansions fail. An implementation of the spectral collocation method rapidly becomes prohibitively cumbersome as standard algorithms, designed to work on rectangular domains, are no longer applicable. Implementation using finite differences, as is done in this text, requires careful house-keeping. The geometry of the problem necessitates the use of non-uniform grids, which further complicates the application of difference formulae. Our experience has shown in these circumstances that three point differencing fail to provide sufficient accuracy.

The method of choice for many practitioners is finite elements. There are many well known commercial packages that are available to solve the problem of arbitrarily filled objects in more and more complicated domains with lesser or greater detail e.g. [8]. Instead we choose a different route, and introduce a finite difference method that is tailored to the specific geometry of the problem to hand. This provides us with greater control over the computational method and visibility of the effects of such things as the grid size and spacing on the accuracy of different parts of the solution inside or outside the cylinder. In particular, the method allows us to study the implementation of perfectly matched layers and exposes some of the issues arising from the size and positioning of the PML which would have otherwise been invisible. We believe the same would be true of more complex geometries, or partially embedded objects for example, which could still be studied without the numerical modelling becoming prohibitively expensive or obscure, and where the solution is likely to be even more sensitive to shape and size of the computational domain.

Our starting point, and the subject of the present article, is cylinders for which we shall address a variety of issues, centred around the long and short range classifications of partly filled cylindrical objects, see Fig. 1, using non-destructive testing techniques. After outlining the problem, and our numerical approach, we give a brief study into the effectiveness of the perfectly matched layer method. In particular, we discuss how to minimise the size of the computational domain, and thereby reduce the necessary computational resources, whilst maintaining accuracy. This will briefly include results obtained using the light fluid loading approximation, in which one makes assumptions as to how the background fluid and solid cylinder interact. Under this approximation the equations in the background fluid and cylinder/contents decouple, and the surrounding fluid and PML do not need to be included in the modelling. This leads to a computational problem of greatly reduced complexity; this limit is suitable for partly filled objects in air but performs poorly for submergence in water. Cylinders submerged in water, which are of more practical importance, are then investigated and issues surrounding the classification of fluid filling are made from observations outside or on the cylinder; in particular, we show how the response of the cylinder depends on the amount of filling present. In each case we consider either forcing concentrated at a single point on the cylinder surface, or forcing from infinity via an incoming plane. These model situations when the structure can be interrogated either directly or only remotely. We conclude by suggesting extensions of this study including the transient problem and stratified fluid fillings.

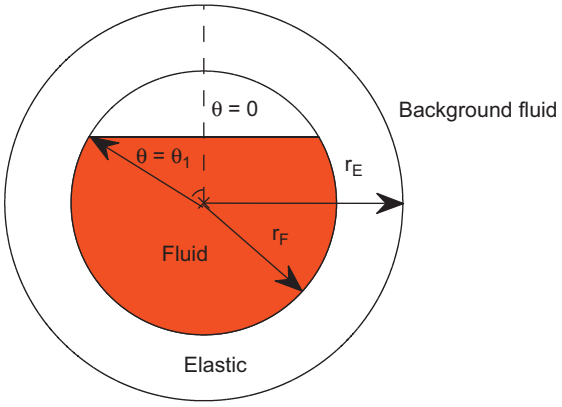

Fig. 1. Polar coordinates centred on the cylinder axis with $\theta = 0$ pointing directly upwards. When we model a background fluid, the computational domain also includes a layer of fluid and a region of perfectly matched layer (PML).

2. Formulation

2.1. Basic equations

We consider an isotropic homogeneous elastic annulus E, occupying the region $r_F < r < r_E$, and assume it is partially filled with an ideal acoustic fluid F, as shown in Fig. 1. When considering submerged cylinders, an ideal fluid B occupies the region $r_E < r < \infty$. The extension of this geometry to partially embedded objects would follow in a similar way. Throughout we shall use j in subscript to denote a parameter of material j, where $j = F, E, B$.

The usual equations for linear elasticity and ideal fluids (e.g. [13]) will apply:

$$\mu_E \nabla^2 \mathbf{u} + (\lambda_E + \mu_E)\nabla(\nabla \cdot \mathbf{u}) = \rho_E \frac{\partial^2 \mathbf{u}}{\partial t^2}, \quad \lambda_j \nabla(\nabla \cdot \mathbf{u}) = \rho_j \frac{\partial^2 \mathbf{u}}{\partial t^2}, \tag{1}$$

where $\mathbf{u}$ is used for displacement here (and henceforth), ρ_j is density for $j = F, E, B$, and λ_E, μ_E, and λ_j for $j = F, B$ are the Lamé parameters for the elastic and two (inner and outer) fluids respectively. Only time-harmonic motions are considered, and the multiplicative factor $\exp(-\mathrm{i}\omega t)$ is considered understood and suppressed henceforth.

We impose continuity of normal displacement and of normal stress across interfaces between fluid and elastic materials. For cases of less than fully filled cylinders, the free-space is assumed to be effectively in vacuo and so stress-free conditions are taken on regions of the inner surface of the elastic annulus not in contact with fluid.

2.2. Perfectly matched layers

To model the infinite outer fluid domain B, we employ a perfectly matched layer (PML) [12]. We limit the physical domain of the outer fluid to $r = r_B$ and introduce the PML within $r_B < r < r_P$ under the following coordinate transformations in this region:

$$r \to r + \frac{\mathrm{i}}{\omega}\int_{r_B}^{r} \alpha(s)\,\mathrm{d}s, \quad \frac{\partial}{\partial r} \to \frac{1}{S}\frac{\partial}{\partial r}, \tag{2}$$

$$h_\theta \to r + \frac{\mathrm{i}}{\omega}\int_{r_B}^{r} \alpha(s)\,\mathrm{d}s \quad \text{where } S(r) = 1 + \frac{\mathrm{i}\alpha(r)}{\omega}, \tag{3}$$

$$\alpha(r) = \alpha_{\max}(r - r_B)^2/(r_P - r_B)^2 \tag{4}$$

in which h_θ is the scale-factor of the coordinate system; the scale-factor for r is unchanged from that of polar coordinates, $h_r = 1$. The choice of decay function $\alpha(r)$ avoids numerical reflection from the PML-fluid boundary and obtains maximum dissipation power [14]. Introducing the potential ϕ_j, defined by $\nabla\phi_j = \partial\mathbf{u}/\partial t$, and applying this transformation yields the following equation for ϕ_B within the PML:

$$\frac{1}{S^2}\frac{\partial^2 \phi_B}{\partial r^2} + \left(\frac{1}{h_\theta S} - \frac{1}{S^3}\frac{\mathrm{d}S}{\mathrm{d}r}\right)\frac{\partial \phi_B}{\partial r} + \frac{1}{h_\theta^2}\frac{\partial^2 \phi_B}{\partial \theta^2} + \eta_B^2 \phi_B = 0, \tag{5}$$

where $\eta_B = \omega/c_B$ and $c_j = \sqrt{\lambda_j/\rho_j}$ for $j = F, B$ are the wavespeeds in the fluid. The choice of a decay function with $\alpha|_{r=r_B} = \mathrm{d}\alpha/\mathrm{d}r|_{r=r_B} = 0$ means that (5) reduces to the equation of motion within the fluid at the interface of the PML and physical domain, $r = r_B$.

2.3. Far field

To model forcing from the far field the formulation is modified slightly by specifying the incoming pressure field in the outer fluid as a plane wave with unit amplitude at angle $\theta = \chi$. The potential in the outer fluid ϕ_B is split into an incoming solution ϕ_{BI} and a scattered solution ϕ_{BS} in the normal way:

$$\phi_B = \phi_{BI} + \phi_{BS} \quad \text{where } \phi_{BI} = \mathrm{i}\exp(\mathrm{i}r(\omega\eta_B)[\cos(\theta - \chi)]). \tag{6}$$

The full solution and, in particular, the field in the outer fluid, is then reconstructed by summing the incident and resulting scattered fields. In the absence of any sources it is well known that one can compute the outer field by integrating around the solid–fluid interface [15]. If Green's function, $G(r, \theta, r_0, \theta_0)$, satisfies: $(\nabla^2 + (\eta_B\omega)^2)G = 0$ away from $(r, \theta) = (r_0, \theta_0)$, where G has a source singularity, then $\phi_{BS}(r_0, \theta_0)$ can be expressed as an integral around the boundary of the cylinder:

$$\phi_{BS}(r_0, \theta_0) = \int_0^{2\pi} \left(G\frac{\partial \phi_{BS}}{\partial r} - \phi_{BS}\frac{\partial G}{\partial r}\right)\Big|_{r=r_B} \mathrm{d}\theta, \tag{7}$$

where $G = (1/4\mathrm{i})H_0^{(1)}(\omega\eta_B R)$ is 2D free space Green's function, $H_0^{(1)}$ is the Hankel function of order 0, and R is the distance between points (r, θ) and (r_0, θ_0), $R = \sqrt{[r\cos(\theta) - r_0\cos(\theta_0)]^2 + [r\sin(\theta) - r_0\sin(\theta_0)]^2}$.

The solution at any point within the outer fluid domain B can thus be computed by solving the problem numerically to produce values of ϕ_{BS} and $\partial\phi_{BS}/\partial r$ on $r = r_B$, the cylinder surface, and then performing the integral numerically; the

trapezoid rule is well suited to this as it benefits from fast convergence on periodic domains [16]. We only require the computational solution around the boundary $r=r_B$, and to obtain this efficiently we wish to model as little of the outer fluid as possible and later we investigate how small the computational domain can be made.

We also require the far-field solution, as $r\to\infty$, $\phi_{BS}(r_0,\theta_0)\sim r_0^{-1/2}\exp(\mathrm{i}\omega\eta_B r_0)D(\theta_0)$ where $D(\theta_0)$ is the directivity given by

$$D(\theta_0)=\int_0^{2\pi}\left(\tilde{G}\frac{\partial\phi_{BS}}{\partial r}-\phi_{BS}\frac{\partial\tilde{G}}{\partial r}\right)\Bigg|_{r=r_B}\mathrm{d}\theta, \tag{8}$$

where $\tilde{G}(\theta,\theta_0)=-\mathrm{i}\sqrt{1/\pi\omega\eta_B}\mathrm{e}^{-\mathrm{i}\pi/4}\exp(-\mathrm{i}\omega\eta_B r\cos(\theta-\theta_0))$.

3. Computational method

3.1. Gridding the domain

The primary challenge to modelling the response of a cylinder with different levels of filling is to introduce a grid in such a way that one can compute accurate derivatives throughout the domain; it soon transpires that this grid cannot be evenly spaced. The natural coordinate system is polar coordinates, centred on the axis of the cylinder. This constrains all grid points to lie either on rays (lines of constant θ) or on circles (lines of constant r). The special cases of an empty or full cylinder are straightforward; problems in which the amount of filling is arbitrary are solved in two different ways, depending on whether the cylinder is more or less than half full. In each case, we begin by distributing grid points on the free-surface, leading to non-uniform grid spacing in both r and θ directions. We assume that the differencing formulae use m_r and m_θ points in the r and θ directions respectively; in practice, optimal efficiency was obtained with $m_r=m_\theta=5$.

If we consider the less than half filled case, shown in Fig. 2 when the radius of the fluid domain is 1 and the elastic material has been omitted for clarity, a m_r point approximation of r derivatives is formed first on the outermost rays θ_1 and $2\pi-\theta_1$ starting at the point of intersection of the free-surface with the elastic material. Grid points are then added along each of the other rays θ_n, where $\theta_1<\cdots<\theta_n<\pi$, that have been defined by the points on the free-surface. This specifies all grid points within the fluid filling; some care must be taken to ensure that the grid is sufficiently dense everywhere.

The incomplete circle $r=r_n$ contains $2(N-n+1)+1$ points, and in particular, circles $r=r_n$ for $n>N-(m_\theta-1)/2+1$ contain less than m_θ points; on these circles $2(N-n+1)+1<m_\theta$ differencing is employed. No θ-differencing is available at the mid point of the free surface but boundary conditions independent of θ derivatives are imposed here so that θ-derivatives are not required.

Once the grid within the fluid filling has been established, separate grids are needed for the elastic material and, if required, the outer fluid and PML. The grid within the elastic material must contain the same points as on the circle $r=1$ within the fluid-filling-grid, to enable application of interface conditions; thus part of the elastic-grid in the θ-direction is already established. The remainder of the grid in this direction is uniformly spaced; the spacing is taken as large as possible such that it is less than the maximum grid spacing used in the fluid-filling domain. The same grid in the θ-direction is used within the outer fluid and PML domains, and each of these grids are uniformly spaced in the r-direction.

The grid in each material is then re-ordered into a single column vector, and differentiation matrices are then composed to act on this vector using a pre-written algorithm [17]. Particular care must be taken when acquiring the weights for points near the boundaries of the domain in the r-direction and to correctly incorporate the periodicity of the θ coordinate. In the more than half filled case, the centre has been excluded from the grid to avoid the singularity there, and one-sided differences are employed. The boundary and interface conditions are carefully applied using separate equations to enforce them. Further details of the numerical method and procedure can be found in [18]. Numerical checks, such as altering the relative discretization size in the elastic shell and fluid, increasing the gridpoints were employed.

It is worth noting at this stage that using non-zero forcing only at a single grid-point is not advocated, as this can lead to a solution dependent on the number of grid points used. The n-order finite difference approximation to a derivative at point P is equivalent to finding the analytic derivative at P of the unique polynomial, of order at most $n-1$, passing through the n points closest to P. Thus as the grid becomes finer, so the power of the forcing (area under a force–distance curve) decreases, leading to amplitude dependent on number of grid points. To model concentrated forcing, we instead apply

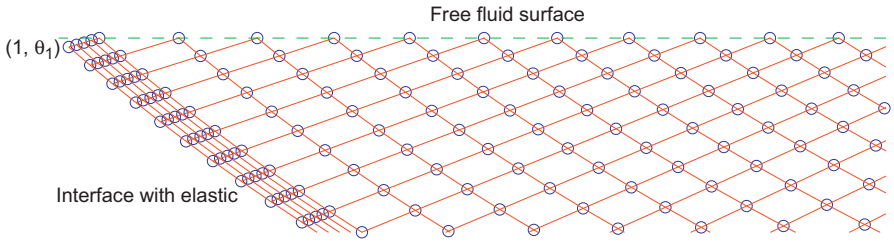

Fig. 2. An example grid for cylinders less than half filled. Nodes are shown as circles, the free-fluid surface is indicated by a dashed curve. The interface with the elastic material is on the left of the figure, although the mesh within the elastic has been omitted for clarity.

forcing with a Gaussian distribution of fixed concentration over a small number of grid points (at least the order of differencing used). Investigation has shown independence of the solution on the number of grid points used and henceforth we refer to this forcing profile as point forcing.

3.2. Minimising the size of the computational domain

We begin by investigating how small one can take the computational domain whilst retaining accuracy; for computational efficiency, one wishes to model the least amount of fluid possible. We consider an acoustically hard cylinder immersed in an infinite fluid, subjected to an incoming plane-wave; an exact analytic series solution is available [9], and is used as a reference solution for comparison. Further, this test problem serves to provide validation of the numerical method employed, in particular the use of the PML.

We suppose a cylinder occupying region $r<1$ is immersed within an infinite ideal acoustic fluid. A potential ψ is defined within the fluid, and taking wavespeed $c=1$ for simplicity, one arrives at

$$(\nabla^2+\omega^2)\psi=0 \text{ for } r>1, \quad \frac{\partial\psi}{\partial r}=0 \text{ on } r=1. \tag{9}$$

We split the field into an incoming and scattered solution: $\psi=\psi_I+\psi_S$, where $\psi_I=\exp(\mathrm{i}\omega r\cos(\theta))$, is an incoming plane wave at angle 0. It follows that $\partial\psi_S/\partial r|_{r=1}=-\mathrm{i}\omega\cos(\theta)\exp(\mathrm{i}\omega\cos(\theta))$ on the surface of the cylinder, and hence the directivity of the scattered far field, $D(\theta_0)$ can be computed using (8), provided $\psi_S|_{r=1}$ can be found computationally. The directivity can also be found directly from the series solution, which we denote $\tilde{D}(\theta_0)$. We define the error between computational and exact solutions as

$$\text{error}=\max_{0<\theta_0<2\pi}|D(\theta_0)-\tilde{D}(\theta_0)|/\max_{0<\theta_0<2\pi}|\tilde{D}(\theta_0)|. \tag{10}$$

The motivation for this choice is to avoid giving misleadingly large errors near points of small amplitude; this would be the case if we simply computed the relative error throughout and took the maximum over $0\le\theta_0<2\pi$.

We then model an annulus of fluid occupying $1<r<R$, so that the length of the fluid domain is $L=R-1$, and a perfectly matched layer one wavelength long. The number of points per wavelength, the key criterion in determining the accuracy of the difference scheme, is held constant to avoid any bias within the results. We aim to establish how much surrounding fluid, if any, must be modelled to obtain an accurate solution. It is worth noting that various authors model the infinite fluid with PML directly attached to the cylinder surface [19].

Fig. 3 shows the error made by the computational solution as a function of the length of the fluid domain, L, divided by the wavelength, $\lambda=2\pi/\omega$, for frequencies $\omega=1,4,10$. When the PML is taken either on or close to the surface of the cylinder, large errors are observed in the computed far field solution at all frequencies shown. As more fluid is modelled, the errors decrease and, at some frequency dependent value, become much less dependant on domain length. We conjecture that the appearance of these errors is closely connected with creeping waves [20]. A creeping wave within the fluid is one localised to the vicinity of the cylinder, and which decays exponentially with perpendicular distance. The problem of waves running around elastic shells submerged in fluid has been widely studied e.g. [21,22] and it is well known that the wave does not exist in an infinite fluid region in the absence of obstacles, which is what the PML is modelling. The addition of a PML will not poison the solution, provided the creeping wave has amplitude comparable to the numerical error as it enters the layer, however if this assumption is violated we should no longer neglect the creeping wave and errors are introduced as a result of doing so.

By transforming the series solution into an integral [20] it can be shown that the creeping wave decays into the outer fluid: the solution is exponentially small at a perpendicular distance of $\mathcal{O}([\omega/c]^{-1/3})$ from the cylinder. Thus L/λ is required to be at least $\mathcal{O}(\omega^{2/3}/c)$ for an accurate model, which corresponds with the observation from Fig. 3 that errors level off by

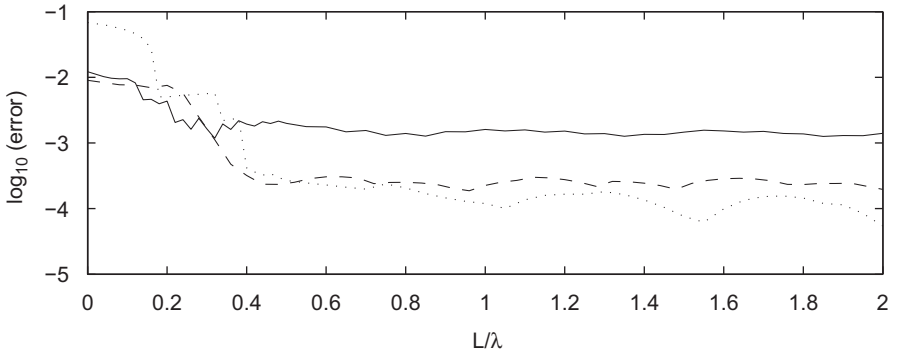

Fig. 3. Error, (10), made by the computational solution, as compared to the analytic series solution, for frequencies $\omega=1,4,10$ shown by solid, dashed and dotted lines respectively for varying amount of fluid included in the model.

$L/\lambda \sim (3/2)[\omega/c]^{2/3}$. As a result of these findings we henceforth impose that the outer fluid domain in the following computations has $L=(3/2)\lambda[\omega/c]^{2/3}$, to ensure sufficient decay of the creeping wave before entering the PML, whilst minimising the size of the computational domain.

The complexity of the problem can be reduced further by using the light fluid approximation [23] whenever it is applicable, that is, if the cylinder is submerged in air. Here, the density of the outer fluid $\rho_B \to 0$ whilst the wavespeed $c_B=(\lambda_B/\rho_B)^{1/2}$ is held constant, and the equations governing the outer fluid decouple from the elastic and filling, allowing us to solve only the elastic/filling problem computationally. This negates the complications of modelling the background fluid and perfectly matched layer, and drastically reduces the model size. To apply this approximation it is necessary to replace the field in the outer fluid, for the case of an incoming plane wave, with the sum of the incident field, the field that would be scattered from a rigid cylinder (known analytically [20]), and the unknown scattered field, that is now a correction to the rigid cylinder solution. The forcing on the cylinder then becomes the sum of the incident field and the scattered field from a rigid cylinder, which are both known, and the response of the cylinder can be calculated by solving only the elastic/filling problem, that is, without modelling the outer fluid. One can then reconstruct the field in the outer fluid and the far field directivity using (7) and (8) respectively, together with the resulting displacement field on the surface of the cylinder.

4. Results

To study the sensitivity of the response (scattered far-field directivity or displacement of the elastic cylinder) of the cylinder to the level of filling, results are provided in this section for combinations of cylinders and different levels of filling, together with variations in incoming and/or observation angle. In particular, we are interested in how the response changes with the level of filling, and in the usefulness, or otherwise, of the response to estimate the nature and level of filling based on short or long-range observations.

In all results presented in this section, five point differencing is used in both r and θ directions. All point forces are applied in a time harmonic manner as described in the formulation in Section 2. Outer and inner radii of the cylinder in question are $r_E=1$ m and $r_F=0.9$ m respectively. For illustration we have chosen the fluid filling to be glycerine, which has $c_F=1860\,\mathrm{m/s}$, $\rho_F=1258\,\mathrm{kg/m^3}$; the elastic material is taken to be steel, with parameters $c_L=5960\,\mathrm{m/s}$, $c_T=3260\,\mathrm{m/s}$, $\rho_E=7700\,\mathrm{kg/m^3}$. Similar commentary to that presented below would follow for other combinations of materials or size and thickness ratio, but is not included explicitly here.

The light fluid approximation can be used when the cylinder is immersed in air, or another gas, and then performs very well, however, for cylinders immersed in water the approximation is poor and we only illustrate it in Fig. 6.

We begin by considering a partly filled cylinder in vacuo where a point harmonic force is applied normal to the cylinder's outer surface, at $r=1$, $\theta=0$ such that the displacement at the point of impact is unity. Fig. 4(a) shows how the response of the cylinder evolves as the quantity of filling changes; the positions of the resonant frequencies observed in the normal displacement at the outer surface of the cylinder are plotted for different levels of filling between empty and completely filled. Filling quantity is measured here and henceforth by volume: a cylinder 1/3 full is taken to mean 1/3 of the region $0\le r<r_F$ is occupied by filling. The exact nature of the response depends on where at the surface the displacement is measured, but the maxima in displacement (plotted in Fig. 4) are observed at the same discrete set of frequencies.

A very fine discretization of the frequency spectrum is required to resolve resonances effectively, due to the strong localisation of responses, and identification by scanning through a range of frequencies and identifying maxima is thus computationally intensive. Strong responses at a discrete set of resonance frequencies are also observed in the far field.

There is a form of resonance mode repulsion shown in Fig. 4: modes look set to cross but then repel one another, a phenomena observed in a wide variety of situations, for example in dispersion curve analysis [4]. With this information, one could imagine measuring the acoustic response of a cylinder whose properties were known *a priori* and so estimate the quantity of filling, or discriminate between objects that were not empty or completed filled. This example shows that the sensitivity of the response to the quantity of filling increases with frequency. In practice, it would be necessary to optimise the frequency bandwidth that was measured in order that the acoustic wavelength was comparable to, or longer than, the size of the object (so that energy can readily penetrate) but also still sensitive to filling.

We demonstrate how the resonances shift as the filling quantity changes by choosing two points to investigate. Panel (a) of Fig. 4 shows two vertical dashed lines at our points of investigation, at filling quantities of 10 percent and 20 percent. We highlight the tenth mode by circles, as this mode undergoes the most rapid evolution of those plotted. Panel (b) shows a portion of the amplitude–frequency curves for our points of investigation, for 10 percent filling (solid curves) and 20 percent filling (dashed curves), and an arrow is drawn to indicate that mode circled in panel (a). It is worth bearing in mind that it is important for the modelling to incorporate this filling, and other modelling, in the absence of filling, or in approximating the filling to empty or completely filled, would no longer be representative of the response of the object.

In the previous example, point forcing was applied at angle $\theta=0$, atop of the cylinder. We note that when the position of the point forcing is changed, the response of the cylinder does not change greatly. The analogue of the previous figure in the case of forcing at $\theta=\pi$ has lower, flatter, resonance modes in identical positions and only slightly perturbs the positions of the higher modes. This further emphasises the aforementioned point that the resonance frequencies of the

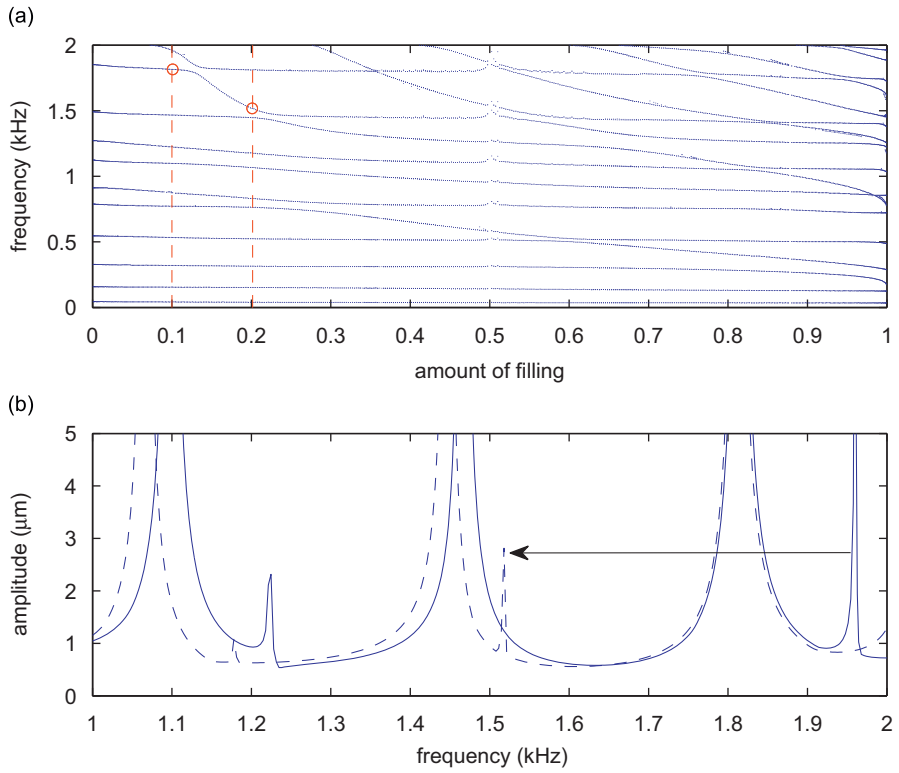

Fig. 4. (a) Evolution of resonance frequencies as the quantity of filling in the cylinder changes. Two such resonances are circled and their frequency–amplitude (maximal normal displacement) curves are shown in panel (b), with solid curves (10% filling) and dashed curves (20% filling). We draw attention to a mode whose resonance moves significantly between these values, shown by an arrow in (b). This is for a part-filled cylinder in vacuo.

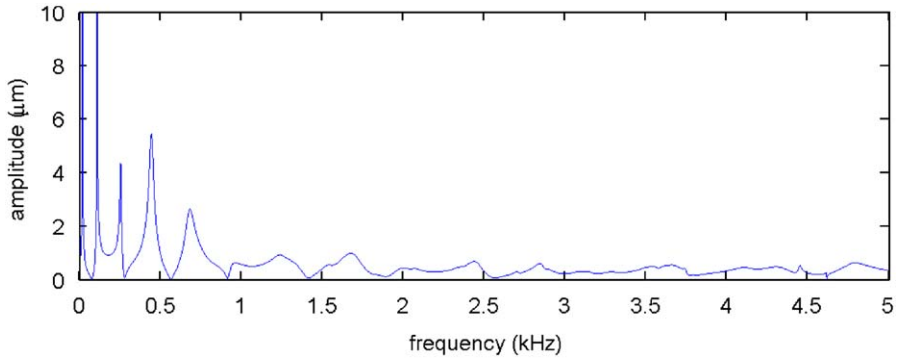

Fig. 5. Response (normal displacement) on the surface of a partly filled cylinder, submerged in water, at $\theta = \pi/3$, when forced at $\theta = 0$. This is for the specific case of $\frac{2}{3}$ filling.

structure are largely independent of locations of measurement and forcing. We note also that tracking resonance frequencies offers no insight into the relative strengths of those resonances, nor how that strength varies with the quantity of filling. For example, the response of the seventh resonance (at ~ 1.3 kHz for the empty cylinder) is very much weaker than resonances pictured at ~ 1.1, ~ 1.45 and ~ 1.8 kHz in Fig. 4(b), but is stronger for fillings greater than ~ 25 percent (not shown here).

When the cylinder is submerged in a fluid, such as water, the relationship between the response and the level of filling appears unchanged; similar behaviour has been observed for objects completely buried in the ground or sediment or otherwise embedded in another medium [24]. However, the strength of the resonant frequencies is vastly diminished; the surrounding fluid serves to damp the response from the cylinder and, in particular, the response at high frequency, so that lower frequencies would need to be utilised, for example, in any characterisation of classification [25]. To illustrate this, Fig. 5 shows the response of a cylinder, $\frac{2}{3}$ full, immersed in water ($c_B = 1421$ m/s, $\rho_B = 1000$ kg/m^3) forced on the outer surface at $\theta = 0$. The point of measurement is on the cylinder surface at $\theta = \pi/3$ and the force amplitude is such that the displacement at the point of impact is unity.

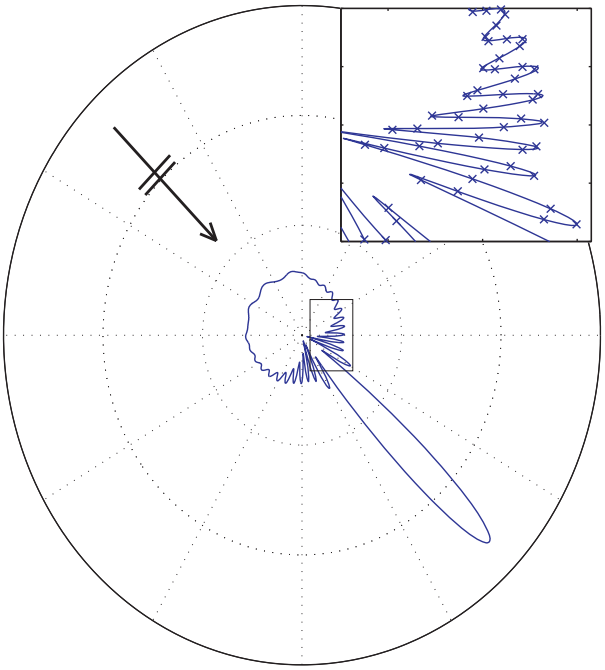

Fig. 6. The magnitude of the far field directivity, $|D|$ (8), for a cylinder $\frac{2}{3}$ full, immersed in air, and irradiated by an incoming plane wave at $\theta = \pi/4$. A comparison between the light fluid approximation (solid curves) and the full model (dashed curves) is presented; the quality of the agreement means the dashed curves lie wholly beneath the solid curves. The inset shows the light fluid solution as a solid curve, and crosses indicate the results of the full solution. An arrow on the figure indicates the direction of the incoming wave.

We now turn our attention to the scattered far field directivity (8) and then the total field inside and outside the cylinder. Fig. 6 shows the far field directivity for a cylinder, $\frac{2}{3}$ full, immersed in air, and irradiated by a 1 kHz incoming plane wave at angle $\theta = \pi/4$. We take this opportunity to compare results obtained using the light fluid approximation to those from the full model, which is discussed in the next section. Results from the light fluid approximation are shown as solid curves, and those obtained using the full model are shown as dashed curves; though indistinguishable on the figure. The inset shows a zoom of the centre of the figure, and a selection of data points extracted from the full solution are plotted as crosses. The agreement is excellent, with a maximum relative error of 0.58 percent. The equivalent comparison in the submerged case yields poor results, as noted previously.

For problems in which plane wave forcing is utilised one may be interested in measuring the scattered far field at some set of discrete angles around the cylinder, not necessarily limited to the angle of plane wave incidence. It is evident in Fig. 6 that there is a discrete set of angles at which the far field amplitude has a maxima, including a large response in the forward direction, though this is more apparent at higher frequencies. Classification of those angles may provide further characteristic traits of the cylinder under investigation, and one may be able to infer an optimal choice of angle.

Figs. 7 and 8 show the displacement and energy density field respectively of a submerged cylinder subjected to a 2 kHz incoming plane wave at an angle $\chi = \pi/4$. The filling and a portion of the fluid surrounding the cylinder, which is $\frac{2}{3}$ full, are also shown. An arrow is pictured to indicate the direction of incidence of the incoming plane wave. The energy plot shows that most of the energy is reflected back into the fluid, contained within $\pi/2$ of the incidence angle, and that a shadow region is observed at $\theta = 5\pi/4$. The figure also demonstrates that very little of the energy is transmitted into the filling of the cylinder.

In practice when classifying an object by measuring it remotely, it is typically the case that one is only able to measure the response in the far field at a few, discrete, points; often including the angle of forcing. We consider cases in which the angle of the incoming plane wave, χ, and the angle at which the far field is measured, θ, are the same. Fig. 9(a) shows the far field response across a spectrum of frequencies for $\theta = \chi = \pi/4$ for a cylinder $\frac{2}{3}$ full. There are a number of points at which the directivity achieves minima, at which points it has discontinuous first derivative; these emerge as resonance frequencies of the structure. We observed that away from such sharp minima, the response varies little with angle of forcing/measurement, however investigation at these special frequencies shows strong dependence on χ.

We present two examples in panels of Figs. 9(b) and (c). Panel (b) shows the far field observed at $\theta = \chi$ for all $0 \leq \chi < 2\pi$ in the case when such a minimum occurs, at 2 kHz, circled in panel (a). This plot should not be confused with Fig. 6, in which the cylinder was irradiated from a fixed angle and the resulting directivity was found for all θ. There are a number of angles at which the directivity is large, and a minimum is observed at $\theta = \pi/3$. By contrast results in panel (c), observed at a maximum at 2.6 kHz, also circled in panel (a), show very little variation with χ. At this frequency, the position chosen to

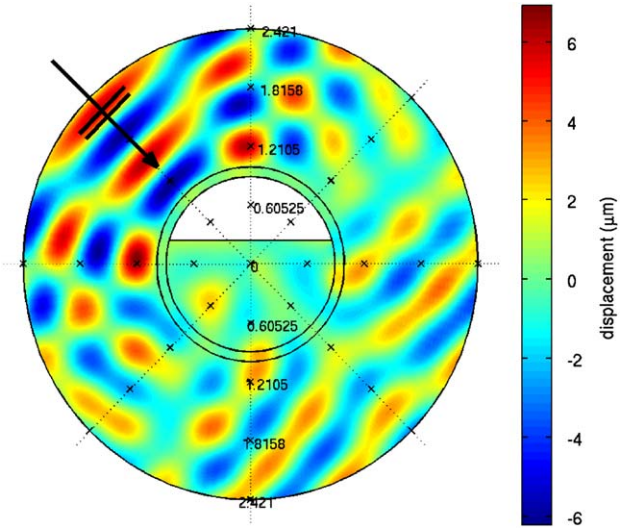

Fig. 7. (Colour online) The displacement field of a cylinder $\frac{2}{3}$ full, submerged in water, subject to a 2 kHz incoming plane wave at an angle $\theta = \pi/4$.

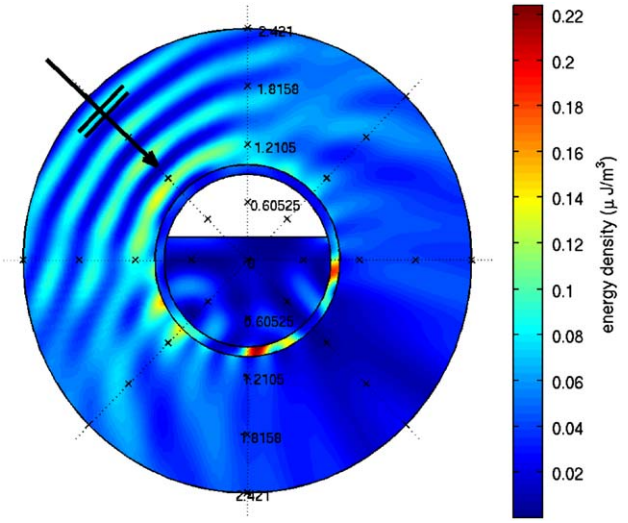

Fig. 8. (Colour online) The energy density of a cylinder $\frac{2}{3}$ full, submerged in water, full subject to a 2 kHz incoming plane wave at an angle $\theta = \pi/4$.

force and measure the cylinder is irrelevant; there are no preferred directions as in panel (b). This phenomena was not limited to the maxima, but observed at all frequencies away from the resonances observed in panel (a).

5. Conclusions

The response of submerged and partially filled cylindrical structures to different levels of filling has been studied in this paper; such problems are potentially useful in detecting and characterising underwater objects including long range testing. We have introduced and outlined a new computational method to model the non-uniform domains needed to address arbitrarily filled cylinders. We have carefully discussed the use of perfectly matched layers in cylindrical coordinates and discovered that care needs to be taken with their application, in particular with regard to whether these layers can be placed very close to the cylinder surface. An adequate distance away from the surface is necessary to ensure that elements of the physical solution are preserved, in particular the creeping wave that propagates into the shadow region of the cylinder.

We have provided results for a set of problems, including point and plane wave forcing, on cylinders immersed in different fluids, and offered a discussion on the relationship between the resonances that are observed and the level of filling. In all cases, strongly localised responses occur, and in the future these could provide an avenue through which the inverse problem could be tackled e.g. to infer how much filling is present. However, large responses are not always evident,

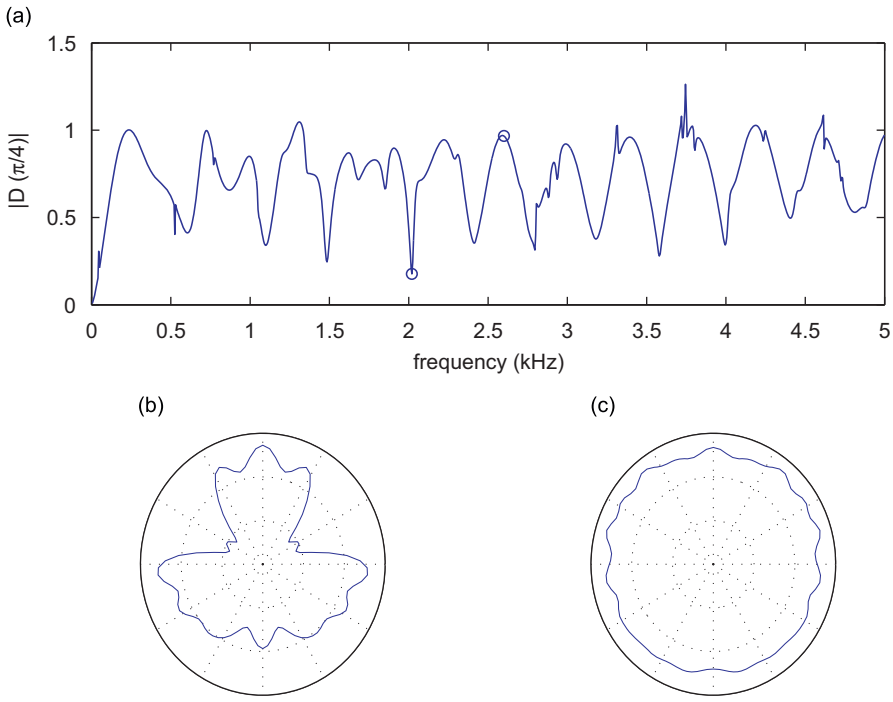

Fig. 9. A cylinder which is $\frac{2}{3}$ full, and submerged in water, is irradiated by an incoming plane wave applied at angle χ, and the magnitude of the far field directivity, (8), is measured at $\theta = \chi$ (incidence angle). Panel (a) shows the variation of the absolute value of directivity with frequency for $\chi = \pi/4$, and panels (b) and (c) show $|D|$ for all $0 \leq \chi < 2\pi$ at the specific frequencies 2 kHz (resonance) and 2.6 kHz (off resonance) respectively, both of which are circled in panel (a). At resonance, there is strong variation in response with χ, however off resonance the variation is insignificant.

for example, when the cylinder is forced from the surrounding fluid, and this is likely to complicate any effort to classify or characterise the object.

One could readily extend this work to include an investigation into how the response of the structure varies with different materials. If, for example, the cylinder dimensions are known, and it is known *a priori* that the cylinder contains one of a limited number of fluids, testing each situation separately is expected to yield characteristic responses of the materials. Otherwise, the response could also be tested for the nature of the filling.

We chose at the outset to fix parameters, such as the nature of the fluid filling and the cylinder dimensions/material, to present a clear picture of how responses vary with quantity of filling. However there are numerous ways in which one could utilise the method contained herein to extend this work. The transient problem could be readily approached: the choice of mesh, and spatial differentiation matrices required are unchanged, and the only difference is the requirement to implement a time-stepping routine to Eq. (1). Alternatively, investigation into a stratified fluid would require only that the equation governing the filling be changed. Modelling a layered fluid would require some modification to the gridding algorithm. One would need to impose that grid points lay along fluid interfaces and continuity conditions hold, however after such changes, generation of differentiation matrices would be straightforward, as the same weight-formulae would apply.

Acknowledgements

This work has been carried out in the Mathematics Department of Imperial College London and Platform Sciences Group of Dstl Physical Sciences. We acknowledge support from the EPSRC and CASE MoD DSTL studentship awarded to Samuel Adams. This paper contains Crown copyright material.

References

[1] J.A. Bucaro, B.H. Houston, M. Saniga, L.R. Dragonette, T. Yoder, S. Dey, L. Kraus, L. Carin, Broadband acoustic scattering measurements of underwater unexploded ordnance, *J. Acoust. Soc. Am.* 123 (2008) 738–746.
[2] X.L. Bao, P.K. Raju, H. Überall, Circumferential waves on an immersed fluid-filled elastic cylindrical shell, *J. Acoust. Soc. Am.* 105 (1999) 2704–2709.
[3] R.D. Doolittle, H. Überall, Sound scattering by elastic cylindrical shells, *J. Acoust. Soc. Am.* 39 (1966) 272–275.
[4] H. Überall, Acoustics of shells, *Acoust. Phys.* 47 (2001) 115–139.
[5] J.A. Fawcett, Scattering from a partially fluid-filled elastic-shelled sphere, *J. Acoust. Soc. Am.* 109 (2001) 508–513.

[6] V.F. Humphrey, N. Jayasundere, M. Dench, P.A. Chinnery, FE modelling of scattering by partially fluid-filled cylindrical shells, *Proc. Inst. Acoust.* 27 (2005) 175–185.
[7] P.B. Goncalves, R.C. Batista, Frequency response of cylindrical shells partially submerged or filled with liquid, *J. Sound Vib.* 113 (1987) 59–70.
[8] M. Zampolli, F.B. Jensen, A. Tesei, Benchmark problems for acoustic scattering from elastic objects in the free field and near the seafloor, *J. Acoust. Soc. Am.* 125 (2009) 89–98.
[9] L.B. Felsen, N. Marcuvitz, *Radiation and Scattering of Waves*, Wiley Interscience, New York, 1972.
[10] E.A. Skelton, J.H. James, *Theoretical Acoustics of Underwater Structures*, Imperial College Press, London, 1998.
[11] J.A.C. Weideman, S.C. Reddy, A MATLAB differentiation matrix suite, *ACM Trans. Math. Software* 26 (2000) 465–519.
[12] J.P. Berenger, A perfectly matched layer for the absorption of electromagnetic waves, *J. Comput. Phys.* (1994) 185–200.
[13] J.D. Achenbach, *Wave Propagation in Elastic Solids*, North-Holland, Amsterdam, 1973.
[14] E.A. Skelton, S.D.M. Adams, R.V. Craster, Guided waves in perfectly matched layers, *Wave Motion* 44 (2007) 573–592.
[15] C.M. Linton, P. McIver, *Handbook of Mathematical Techniques for Wave/Structure Interactions*, Chapman & Hall, UK, 2001.
[16] L.N. Trefethen, *Spectral Methods in MATLAB*, SIAM, Philadelphia, 2000.
[17] B. Fornberg, Calculation of weights in finite difference formulas, *SIAM Rev.* 40 (3) (1998) 685–691.
[18] S.D.M. Adams, Asymptotic and Numerical Methods for Surface Waves and Modes in Elastic Guiding Structures, PhD Thesis, Imperial College London, 2009.
[19] M. Zampolli, A. Tesi, F.B. Jensen, A computationally efficient finite element model with perfectly matched layer applied to scattering from axially symmetric objects, *J. Acoust. Soc. Am.* 122 (2007) 1472–1485.
[20] D.S. Jones, *Acoustic and Electromagnetic Waves*, Oxford Science Publications, Oxford, 1986.
[21] G.C. Gaunaurd, Elastic and acoustic resonance wave scattering, *Appl. Mech. Rev.* 42 (1989) 143–192.
[22] C.W. Horton, M.V. Mechler, Circumferential waves in a thin walled air filled cylinder in a water medium, *J. Acoust. Soc. Am.* 51 (1972) 295–303.
[23] R.V. Craster, The light fluid loading limit for solid/fluid interaction, *Eur. J. Appl. Math.* 8 (1997) 484–505.
[24] A. Tesei, J.A. Fawcett, R. Lim, Physics based detection of man-made elastic objects buried in high-density-clutter areas of saturated sediments, *Appl. Acoust.* (2008) 422–437.
[25] D. Décultot, K. Cacheleux, G. Maze, Detection and classification of an object buried in sand by an acoustic resonance spectrum method, *Proc. Inst. Acoust.* 29 (2008) 162–169.